scientific reports

Check for updates

OPEN

Piezo1 knockdown activates PI3K/AKT and enhances SPP1 to drive M2 macrophage polarization and reduce cardiac inflammation

Yunhan Zhang[1,6], Ying Zhang[2,6], Jiaoyan Song[3,6], Ziwen Zhao[1,6], Wenhao Ju[4], Hao Zhang[4], Shuang Li[1], Hanlu Li[4], Qiuzhe Guo[1], Yinbo Ma[4], Zhangwei Nong[4], Tianyuan Shen[1], Yuanzheng Wang[1], Boheng Pang[4], Min Hao[1], Chunyuan Luo[1], Zhiling Luo[1]✉, Yinjiang Tang[1]✉, Donglin Zhuang[4]✉ & Jianqiu Pei[5]✉

Piezo1 plays a key role in the immune response during sepsis. To date, our understanding of the role of Piezo1 in inflammatory diseases has mostly been limited to influencing vasomotor function and regulating inflammatory infiltration. Whether and how Piezo1 in macrophages is involved in developing septic cardiac dysfunction has never been explored. Here, we have successfully established a mouse model with myeloid cell-specific knockdown of Piezo1. The intraperitoneal injection of lipopolysaccharide (LPS) resulted in a significant increase in cardiac macrophage infiltration, as well as an increase in the expression of inflammatory factors and the inflammatory response. However, myeloid cell-specific knockdown of Piezo1 impaired this response, leading to an increase in macrophage polarization towards the M2 type and the decreased inflammatory response. As a result, myocardial injury caused by sepsis was attenuated. We have also demonstrated that the PI3K/AKT pathway is significantly activated after Piezo1 knockdown, resulting in reduced myocardial dysfunction. Our data indicate that myeloid cell-specific knockdown of Piezo1 can influence macrophage polarization and thus exert cardioprotective effects in a murine model of sepsis, providing potential ideas and targets for the treatment of infectious cardiac dysfunction.

Keywords Piezo1, Macrophage, Sepsis-induced cardiomyopathy, Cardiac dysfunction, PI3K/AKT pathway

Abbreviations

LPS	Lipopolysaccharide
SCM	Sepsis-induced cardiomyopathy
IL-6	Inflammatory cytokines like interleukin 6
TNF-α	Tumor necrosis factor-alpha
IL-1β	Interleukin 1β
cTnI	Cardiac troponin I
WGA	Wheat germ agglutinin
IACUC	Institutional Animal Care and Use Committee
RT-qPCR	Real-time quantitative PCR

[1]The Department of Ultrasonography, Fuwai Yunnan Hospital, Chinese Academy of Medical Sciences/Affiliated Cardiovascular Hospital of Kunming Medical University, Kunming 650102, China. [2]The 4th Healthcare Department of the Second Medical Center, Chinese PLA General Hospital, National Clinical Research Center for Geriatric Diseases, Beijing 100853, China. [3]Department of Endocrinology, Key Laboratory of Endocrinology of National Health Commission, Translation Medicine Centre, Peking Union Medical College Hospital (PUMCH), Peking Union Medical College (PUMC), Chinese Academy of Medical Sciences (CAMS), Beijing 100730, China. [4]Department of Structural Heart Disease, National Center for Cardiovascular Disease, State Key Laboratory of Cardiovascular Disease, China and Fuwai Hospital, Chinese Academy of Medical Sciences and Peking Union Medical College, Beijing 102308, China. [5]Department of Biochemistry and Molecular Biology, School of Basic Medical Sciences, Beijing Key Laboratory of Metabolic Disorders Related Cardiovascular Disease, Capital Medical University, Beijing 100069, China. [6]Yunhan Zhang, Ying Zhang, Jiaoyan Song and Ziwen Zhao contributed equally to this work. ✉email: luozhiling@kmmu.edu.cn; tangyinjiang1@126.com; rinrpg@163.com; peijianqiu0620@126.com

HE	Hematoxylin-eosin
BMDMs	Bone marrow derived macrophages
Piezo1-cKO	Piezo1$^{f/f}$Lyz2-Cre
FDR	False discovery rate
DEGs	Differentially expressed genes
GEO	Gene expression omnibus
LVEF	Left ventricular ejection fraction
FS	Fractional shortening
P-AKT	Phosphorylated AKT

Sepsis is a systemic inflammatory response characterized by excessive production of inflammatory cytokines, oxidative stress, and multiple organ dysfunction. One severe sequel of this multiorgan impairment is sepsis-induced cardiomyopathy (SCM), characterized by myocardial depression and ensuing high mortality due to cardiac dysfunction. This condition arises from an overwhelming secretion of inflammatory mediators and chemokines during the septic response, inflicting damage upon myocardial cells[1]. Macrophages are well-known for their pivotal roles in preserving homeostasis, defending against pathogens, and repairing tissue damage[2]. They are capable of differentiating into various functional phenotypes in different environments and tissues. These phenotypes include the classical activation phenotype (M1 type), which exhibits a circular or irregular morphology, has a pro-inflammatory effect, and is associated with the CD86 marker. The alternative activation phenotype (M2 type) displays a slender or fusiform morphology, has a repair effect, and is characterized by the CD206 marker[3–5]. Furthermore, endotoxin, a key component of the outer membrane of gram-negative bacteria and a principal instigator of sepsis, provokes macrophage activation and drives polarization toward the M1 phenotype. This polarization leads to an overproduction of inflammatory cytokines like interleukin 6 (IL-6), tumor necrosis factor-alpha (TNF-α), and interleukin 1β (IL-1β), thereby fueling an inflammatory cascade that exacerbates damage to cardiomyocytes[6], thus leading to an increase in cTnI (cardiac troponin I) levels. cTnI, as a serum marker for diagnosing myocardial injury, possesses high specificity and is not influenced by intense exercise, skeletal muscle injury, or renal disease[7]. Thus, inhibiting macrophage activation is crucial in reducing myocardial injury during sepsis.

Piezo1 is a mechanically activated ion channel with a high affinity for calcium[2]. It is evolutionarily conserved and involved in the development, differentiation, and growth of multiple tissues. It responds to diverse mechanistic stimuli across numerous cell types[8], with a distinctive significance in the regulation of inflammatory infiltration subjected to hemodynamic stress. Activation of the PI3K/AKT phosphorylation pathway is manifested by upregulation of the expression of pathway-associated proteins and upregulation of the phosphorylation level of proteins. Activation of the pathway promotes macrophage polarization to the M2 type, with an increase in the proportion of macrophages of the M2 type and enhanced anti-inflammatory effects[9]. Recent studies have revealed that macrophages demonstrate significant expression of Piezo1, which is pivotal to their involvement in mediating inflammatory responses[10–12].

In this study, we employed a classical sepsis model induced by LPS to investigate the role of Piezo1 in regulating macrophage responses during sepsis[13]. Our research findings suggest that macrophage polarization relies on the function of Piezo1. Following the knockdown of Piezo1, the application of LPS resulted in an enhanced phosphorylation of the PI3K/AKT pathway, concomitant with an upregulation in the expression of SPP1. This shift correlated with an increased polarization of macrophages towards the M2 phenotype, leading to a reduction in myocardial injury. We showed that macrophages lacking Piezo1 holistically reduce inflammation responses. This suggests the regulatory role of Piezo1 and the possibility of Piezo1 as a potential therapeutic target in Sepsis-induced cardiomyopathy.

Materials and methods

Detailed methods are presented in the Supplementary material. The data that support the findings of this study are available from the corresponding author, [J.P], upon reasonable request.

Animals

The mice needed for the experiment were purchased from Shanghai Model Organisms Center, Inc. Wild-type, Piezo1$^{flox/flox}$, and Piezo1$^{flox/flox}$ Lyz2-Cre C57BL/6J mice, all male and aged eight weeks, were maintained in specific pathogen-free environments and sustained on a standard mouse chow diet. The impact and conclusions regarding gender differences in SCM have not yet gained widespread recognition. Consequently, the use of male mice remains the predominant choice. The male mice were intraperitoneally injected with LPS to establish the model of SCM. With a Visualsonics Vevo 3100 ultrasound system (FUJIFILM Visual Sonics Inc., Toronto, Canada), and Wheat Germ Agglutinin (WGA) staining of myocardial tissue was identified. The SCM mouse model was created successfully when decreased myocardial contraction amplitudes and a pronounced augmentation in myocyte edema were observed compared with the control group. The details of myeloid cell-specific Piezo1 knockout mice generation, as well as animal experiments, are presented in the supplemental material.

All animal experiments were done by the Guide for the Care and Use of Laboratory Animals published by the Ministry of the People's Republic of China (1998) and approved by the Institutional Committee on Animal Care of Capital Medical University. The animal research was sanctioned by the Institutional Animal Care and Use Committee (IACUC), under the approval number A5095F17-EA0D-4377-88F7-FED2CE3A2ED2. All methods were performed in accordance with the relevant guidelines and regulations, and followed the ARRIVE guidelines. Genotype is characterized by PCR, and the primer sequences are in Table S1.

Real-time quantitative PCR (RT-qPCR)

Total RNA was isolated from mouse hearts by TRIzol Reagent (Thermo Fisher Scientific, Waltham, MA). At least 1 μg total RNA was used to generate 1st strand cDNA using the DNA (cDNA) Reverse Transcription kit (ThermoFisher Scientific). qRT-PCR was performed with universal SYBR green mix (Cat 172-5122, BioRad) on the StepOne Plus System (Applied Biosystems). Primers were designed for target gene (Piezo1) (forward CCTT CTGTTGCTGGTGTTTG, reverse GTCCTGGTCCAACCTCTGG), reference gene (Gapdh) (forward primer GCACCACCAACTGCTTAG, reverse primer GGATGCAGGGATGATGTTC). Fold changes were calculated by ΔΔCt method. Significance was determined by student's two-tailed t-test, $p < 0.05$.

Echocardiography

Echocardiography was performed on sedated mice under 0.5–1% inhaled isoflurane (IsoFlo Vet; Shenzhen Riwode Life Technology Co., Ltd., Shenzhen, China) anesthesia. A Visualsonics Vevo 3100 ultrasound system (FUJIFILM Visual Sonics Inc., Toronto, Canada) was used for all echocardiographic measurements. Parasternal long-axis and parasternal short-axis views of the left ventricle were obtained in B-mode imaging. The left ventricular motion curve was recorded at the level of the papillary muscles in the M-mode imaging.

Western blot analysis

Protein was extracted from tissue or cell lysates in lysis buffer, a combination of RIPA lysis buffer and a 1% protease inhibitor. The lysate was spun at 14,000 rpm for 15 min, and the supernatant was obtained. The proteins were denatured through the use of LDS sample buffer and sample reducing agent at 70 °C for 10 min before each sample was loaded into a well of a 4–12% Bis–Tris gel (all from Invitrogen). the membrane was then incubated with Piezo1 (Proteintech, 15939-1-AP, 1:500), IL-1β (Proteintech, 26048-1-AP, 1:1000), IL-6 (Cell Signaling Technology, 12153, 1:1000), IL-10RA (Proteintech, 13356-1-AP, 1:1000), Phospho-Akt (Cell Signaling Technology, 5012S, 1:1000), Akt (Cell Signaling Technology, 4685S, 1:1000), Phospho-S6 Ribosomal Protein (Cell Signaling Technology, 5364S, 1:1000), antibodies at 4 °C overnight. Either Peroxidase-Conjugated Goat anti-Rabbit IgG (H + L) (ORIGENE, 2B-2301) was incubated at a concentration of 1:2000, or HRP-conjugated anti-mouse antibody (ORIGENE, 2B-2305) at a 1:5000 dilution was used, depending on the primary antibody requirements provided by the manufacturer. The antibodies are in Table S2. Uncropped blots are provided in the Source Data file.

Histology

Tissue samples were fixed in 4% paraformaldehyde and subsequently embedded in paraffin. Sections of 5 μm thickness in the short axis of the papillary muscle of the left ventricle were cut and then stained with a standard hematoxylin–eosin (HE) staining protocol. Four regions were selected for each slice, and each slice is observed at the same location. Additional sections were blocked by incubating for 30 min in 5% serum in PBS. Primary antibodies were then applied for immunostaining (Table S2). Using ImageJ software to measure the area and intensity of the fluorescent signal, and calculating the ratio of fluorescence intensity to area (e.g., fluorescence intensity/area) to reflect the expression level of the target protein.

Peritoneal macrophage isolation

Macrophages were isolated from the peritoneal fluid of mice. In brief, the mice peritoneum was injected with 3% thioglycollate broth (1 mL) once daily for three days. Euthanizing mice via cervical dislocation post-anesthesia (2.5% inhaled isoflurane) and collecting peritoneal fluid, macrophages were collected by centrifugation (1000 RPM, 5 min) and plated in 75 cm^2 culture flasks. The macrophages were cultured in RPMI-1640 at 37 °C for 2–3 h to allow adhesion; non-adherent cells were washed away with RPMI-1640 and discarded.

Bone marrow derived macrophages isolation

Bone Marrow Derived Macrophages (BMDMs) were isolated from the femurs and tibiae of mice, euthanizing mice via cervical dislocation post-anesthesia (2.5% inhaled isoflurane) and collecting the bones. The femur and tibiae were handled in 75% ethanol on ice, washed in PBS 3x, then flushed out marrow using a syringe. BMDMs were collected using a 70 μm strainer and centrifugation (1500 RPM, 5 min). Red blood cells were removed with red cell lysis buffer (Miltenyi Biotec, #130-107-677). Then plated in 75 cm^2 culture flasks. Isolated BMDMs were cultured in macrophage medium, and the medium was exchanged once every two days until the cells were > 90% confluent (~7 days later).

Flow cytometry

The cells were resuspended with CD16/32 (Biolegend, 101302) after centrifuging at 500 g for 10 min, then incubated on ice for 10 min. Washed in PBS/BSA (PBS pH 7.4 and 1% BSA) Buffer, Anti-F4/80 conjugated with APC (Biolegend, 123122) and Anti-CD86 conjugated with PE (Invitrogen, 12-0862-82) were added to a fixative solution and incubated for 30 min. Washed in PBS/BSA (PBS pH 7.4 and 1% BSA) Buffer, Anti-CD206 conjugated with Alexa Fluor 488 (Invitrogen, 53-2061-82) was added in a membrane-breaking solution, and incubated for another 30 min. The cells were then resuspended in PBS. Subsequently, the sample was analyzed by the BD FACSVerse™ flow cytometer, and the data were analyzed by FlowJo v10.10 software with gating strategies as depicted in Fig. S4. Three repeated experiments were performed to obtain the average.

RNA sequencing analysis

Total RNA was isolated from six samples (BMDMs, isolated from the femurs and tibiae of $Piezo1^{f/f}$ and $Piezo1^{f/f}$Lyz2-Cre (Piezo1-cKO) mice following LPS treatment, n = 3) and subjected to transcriptomic analysis for gene-expression profiling. The total RNA quantity and purity were analysis of Bioanalyzer 2100 and RNA

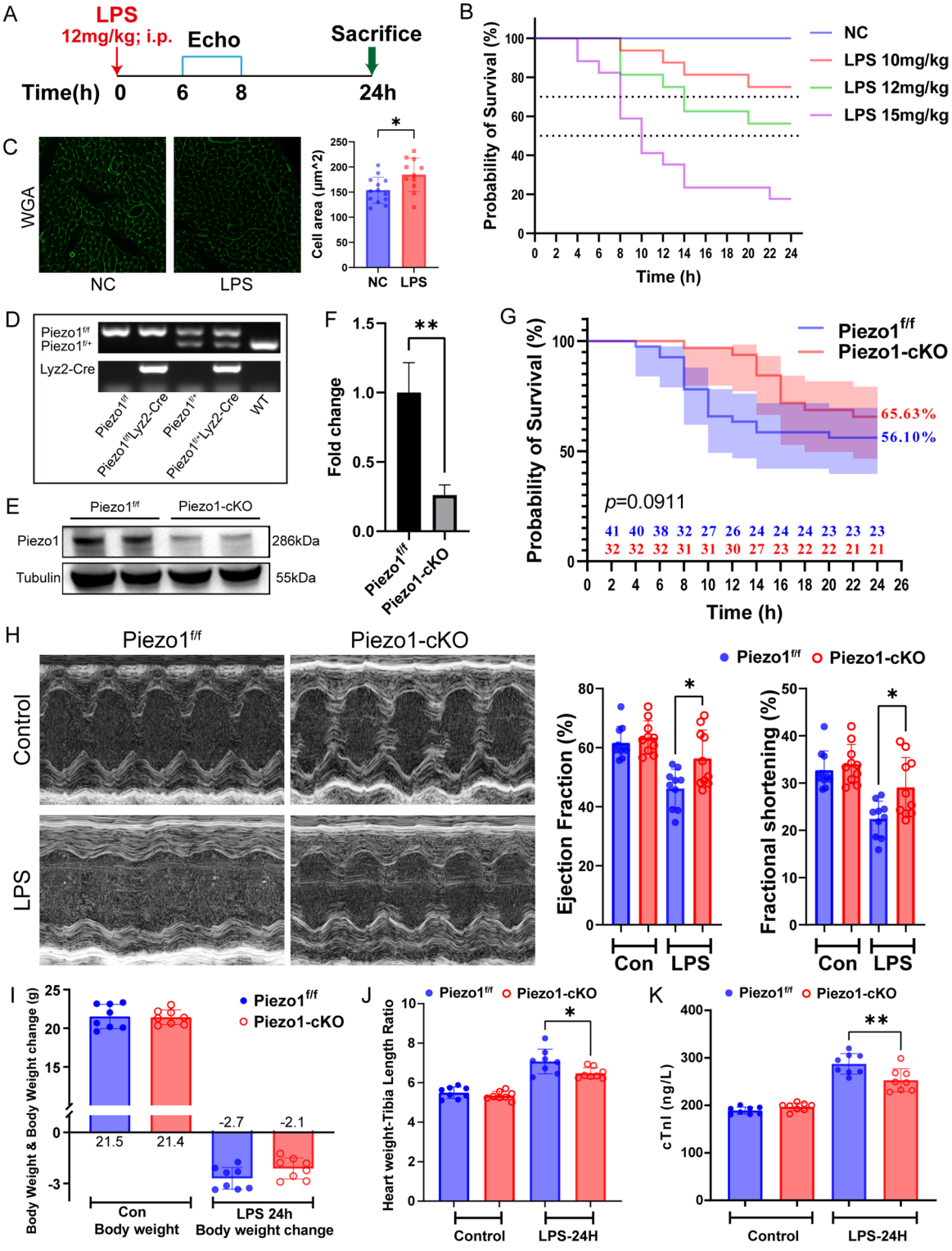

6000 Nano LabChip Kit (Agilent, CA, USA, 5067-1511), high-quality RNA samples with RIN number > 7.0 were used to construct sequencing library. We performed the 2 × 150bp paired-end sequencing (PE150) on an Illumina Novaseq™ 6000. Quality control and mapping onto the mouse reference genome (GRCm39). Genes differential expression analysis was performed by DESeq2 software between two different groups (and by edgeR between two samples). The genes with the parameter of false discovery rate (FDR) below 0.05 and absolute fold change ≥ 2 were considered differentially expressed genes (DEGs), DEGs analysis using Limma R package, and heatmaps creation. Pathway Enrichment Analysis (KEGG) was identified significantly enriched metabolic pathways or signal transduction pathways in DEGs comparing with the whole genome background. Data are available in the Gene Expression Omnibus (GEO) at accession Nos. GSE311976.

◀**Fig. 1**. Construction of sepsis model and pathological indicator alterations in macrophage Piezo1 knockdown mice. (**A**) Schematic representation of the construction of a sepsis model in mice. (**B**) Dose-dependent acute mortality curves in WT mice following LPS induction. (**C**) WGA staining reveals myocardial cell swelling induced by LPS treatment in WT mice (t-test performed for statistical analysis, $p = 0.0178$, n = 13 for negative control, n = 11 for WT mice following LPS induction). (**D**) Genotype identification results for Piezo1$^{f/f}$ and lyz2-Cre transgenic mice. (**E**) Western blot analysis of Piezo1 protein in macrophages from Piezo1 gene knockdown mice before LPS treatment (n = 6). (**F**) Quantitative analysis of Piezo1 protein expression (t-test performed for statistical analysis, $p = 0.0089$, n = 6). (**G**) Comparison of 24-h post-LPS injection survival rates in Piezo1$^{f/f}$ and Piezo1-cKO groups (Kaplan–Meier statistical performed for statistical analysis, $p = 0.0911$). (**H**) Echocardiographic images before and after LPS injection, with comparison of LVEF and FS (one-way ANOVA performed for statistical analysis, Piezo1-cKO vs. Piezo1$^{f/f}$ groups, $p = 0.00128$ for LVEF, $p = 0.00156$ for FS, n = 10). (**I**) Comparison of the degree of weight loss following LPS treatment (one-way ANOVA performed for statistical analysis, $p < 0.001$ for before LPS injection vs. after LPS injection in Piezo1$^{f/f}$ groups, $p < 0.001$ for before LPS injection vs. after LPS injection in Piezo1-cKO groups. $p = 0.9967$ for Piezo1-cKO vs. Piezo1$^{f/f}$ groups before LPS injection, $p = 0.6689$ for Piezo1-cKO vs. Piezo1$^{f/f}$ groups after LPS injection. n = 8). (**J**) Changes in the ratio of heart size to tibial length after LPS treatment (t-test for statistical analysis, $p = 0.00286$ for Piezo1-cKO vs. Piezo1$^{f/f}$ groups after LPS injection, n = 8). (**K**) Alterations in cTnI levels before and after LPS treatment (one-way ANOVA performed for statistical analysis, $p = 0.0022$ for Piezo1-cKO vs. Piezo1$^{f/f}$ groups after LPS injection, n = 8).

Quantification and statistical analysis

All data are representative of at least three independent experiments. All statistical analyses were performed using Prism 9.5.1 (GraphPad). The data are presented as the mean ± SD as indicated in the legends, and comparisons between the two groups were carried out using the t-test. Data analysis on multiple groups was conducted by ANOVA test. Survival data were analyzed by the Kaplan–Meier statistical method. A p-value < 0.05 was considered statistically significant.

Results

Cardiac function decreased in mice with sepsis after LPS stimulation, and this impairment was ameliorated after the knockdown of Piezo1 in macrophages.

To investigate the impact of LPS on cardiac function, we divided male C57BL/6J mice, wild-type and eight-week-old, into 4 groups and administered LPS via intraperitoneal injection at progressive doses of 0 mg/kg (n = 16), 10 mg/kg (n = 16), 12 mg/kg (n = 16), and 15 mg/kg (n = 17). These doses corresponded to survival rates of 100%, 75%, 56.25%, and 17.65% (Fig. 1B). Opting for a dose of 12 mg/kg LPS for our sepsis model, we were able to maintain mouse survival rates at 50–70%. Before LPS injection, baseline cardiac assessments were performed using echocardiography. A follow-up echocardiographic evaluation was conducted 6–8 h post-LPS administration. Cardiac function was quantitatively assessed by recording and analyzing M-mode echocardiograms (Fig. 1A). Our findings indicate that intraperitoneal administration of LPS precipitates myocardial damage. Echocardiographic analysis revealed substantial degradation in cardiac function, with marked left ventricular systolic dysfunction observed notably in the LPS-treated mice (Fig. S1), and Piezo1 levels were notably increased through Western blot analysis in the LPS-treated mice (Fig. S2). This was characterized by decreased myocardial contraction amplitudes and a pronounced augmentation in myocyte edema in the LPS-treated mice (Fig. 1C).

One study has discovered that specific knockout of Piezo1 in macrophages can protect the mouse liver and decelerate the progression of fibrosis[14]. To investigate the role of Piezo1 in sepsis-induced cardiomyopathy, we generated myeloid cell-specific Piezo1 knockdown C57BL/6J mice (Fig. 1D). Piezo1$^{f/f}$ and Piezo1$^{f/f}$Lyz2-Cremice were used, and we first harvested peritoneal macrophages. Through Western blot analysis, we confirmed the effective deletion of Piezo1, ultimately demonstrating a knockdown efficiency of 74% (Fig. 1E and F). We harvested heart of mice, through RT-qPCR analysis, we confirmed the effective deletion of Piezo1 in the mRNA-level expression in Piezo1-cKO mice ($P < 0.0001$) vs. Piezo1$^{f/f}$ mice (Fig. S3).

Then, we constructed a model of sepsis in eight-week-old male Piezo1$^{f/f}$ (n = 41) and Piezo1-cKO (n = 32) mice. The sepsis yielded a survival rate of approximately 65.63% in Piezo1-cKO mice, but only approximately 56.10% of Piezo1$^{f/f}$ mice ($p = 0.0911$) (Fig. 1G). Before administering LPS, Piezo1 knockdown did not exhibit mortality, and there were no significant differences in cardiac function, cardiac mass and body weight between Piezo1$^{f/f}$ and Piezo1-cKO groups (Fig. 1H, I and J). However, following LPS treatment, both Piezo1$^{f/f}$ and Piezo1-cKO groups exhibited a significant reduction in body weight, left ventricular ejection fraction (LVEF), and fractional shortening (FS) ($p < 0.0001$; $p = 0.0001$; $p < 0.0001$, respectively). Notably, the Piezo1$^{f/f}$ group displayed worse cardiac function, with LVEF and FS being significantly lower compared to the Piezo1-cKO group (Fig. 1H, $p = 0.0128$ for LVEF and $p = 0.0156$ for FS). Additionally, the Piezo1$^{f/f}$ group presented with an increased cardiac mass, as evidenced by an elevated heart weight-to-tibia length ratio ($p = 0.0286$) (Fig. 1J). Serological assays also showed a greater increase in cTnI levels in the Piezo1$^{f/f}$ group ($p = 0.0022$) (Fig. 1K).

Our results indicate that targeted knockdown of Piezo1 in macrophages may impart a cardioprotective advantage in septic mice, potentially mitigating mortality rates associated with sepsis-induced cardiomyopathy.

Piezo1 knockdown alleviates myocardial cell damage via induction of M2 macrophage polarization.

First, in the ventricular septal and left ventricle, HE staining revealed disorganized myocardial fibers, partial fiber rupture, and degeneration, with striations becoming blurred or vanishing (vacuolization), interstitial edema, and inflammatory cell infiltration following LPS treatment (Fig. 2A). Furthermore, in the ventricular

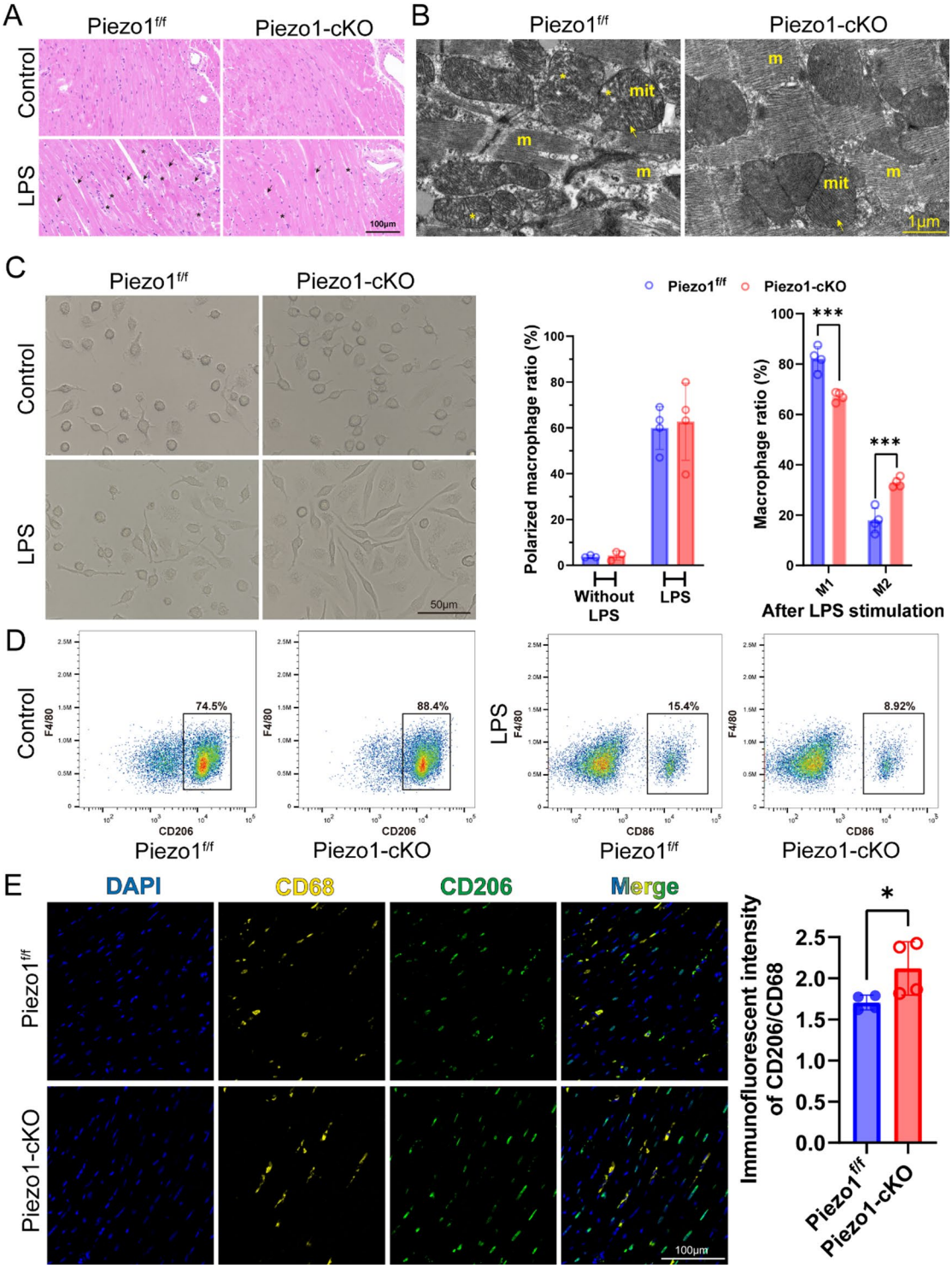

Fig. 2. Cardiac histopathological changes and macrophage characterization. (**A**) H&E staining of cardiac tissues before and after LPS administration, vacuolization of myocytes ("↑") and myofibrillar rupture ("*") (n = 4). (**B**) Electron micrographs of myocardial ultrastructure post-LPS treatment, depicting mitochondria ("mit"), myofibers ("m"), cristae of mitochondria ("↑"), and mitochondrial vacuolation ("*") (n = 4). (**C**) Microscopic imaging of BMDMs along with statistical analysis of typical cell phenotypes (Two-way ANOVA performed for statistical analysis, $p = 0.0002$, n = 4). (**D**) Flow cytometric enumeration of BMDMs (n = 4). (**E**) Fluorescent staining and quantification of CD68 and CD206 in cardiac tissue sections (t-test for statistical analysis, $p = 0.0486$, n = 4).

septal, the transmission electron microscopy revealed disorganized myocardial fibers, myofibrillar separation, twisting of the Z lines, shortened distances between Z lines, disorder of mitochondria within myocardial cell, swelling, diminished mitochondrial cristae, and necrotic changes including partial vacuolization (Fig. 2B). But these damages were significantly mitigated in the Piezo1-cKO group compared to the Piezo1$^{f/f}$ group. Then we isolated bone marrow-derived macrophages for culture, M1 phenotype showed a round and flattened morphology, and M2 phenotype showed elongated morphology. And under the microscope, there was no evident differentiation before LPS treatment. Flow cytometry analysis further confirmed the polarization states of these macrophages using a cell surface marker-based classification. After 36 h of exposure to LPS, the differentiation ratio was around 60%, with no significant difference between the Piezo1$^{f/f}$ and Piezo1-cKO groups ($p = 0.7807$). Based on the morphology of the macrophages, M1 and M2 phenotypes were distinguished: the Piezo1-cKO group exhibited a higher proportion of M2 macrophages among the differentiated cells (32.91% vs. 17.87%, $p = 0.0002$) (Fig. 2C). This was further substantiated by flow cytometry, which identified macrophages with the F4/80 marker and M2 macrophages with the CD206 marker, and identified macrophages with the F4/80 marker and M1 macrophages with the CD86 marker. The Piezo1-cKO group showed a higher ratio of M2 and a lower ratio of M1 macrophages among differentiated cells (M2 is 88.4% vs. 74.5%, M1 is 8.92% vs. 15.4%) (Fig. 2D).

To ascertain if the abundance of M2 macrophages within myocardial tissue paralleled our in vitro observations, we performed fluorescence staining with CD68 and CD206. The Piezo1-cKO group exhibited a stronger CD206 expression ($p = 0.0486$) with cellular morphology more representative of the archetypal M2 macrophage phenotype (Fig. 2E).

We contend that silencing Piezo1 in macrophages induces a skewing toward an M2 anti-inflammatory phenotype, concomitantly diminishing myocardial inflammation and alleviating cardiomyocyte injury, thus safeguarding cardiac functionality.

Macrophage Piezo1 Knockdown Activates the PI3K/AKT Pathway and Promotes M2 Polarization.

To investigate the mechanism by which Piezo1 regulates macrophage polarization, we conducted transcriptomic sequencing. Following LPS treatment, it was found that compared to the control group (LPS-treated Piezo1$^{f/f}$ mice), macrophages with Piezo1 knockdown (LPS-treated Piezo1-cKO) showed significant upregulation in 511 genes and downregulation in 74 genes ($p < 0.05$). The differential gene expression clustering heat map was consistent with these changes (Fig. 3A and B). Notably, as a factor that can drive macrophage polarization toward the M2 phenotype[15–17], the SPP1 gene was also significantly upregulated ($p = 5.3E-07$). Further, KEGG enrichment analysis indicated a significant accumulation of genes related to the PI3K/AKT signaling pathway (Fig. 3C)[18–20]. The Heatmap analysis showed a significant increase in genes related to the PI3K/AKT signaling pathway and anti-inflammatory cytokines IL-10, and a significant decrease in pro-inflammatory cytokines IL-1β and IL-6 (Fig. 3D). To validate the sequencing analysis results, we isolated and cultured bone marrow-derived macrophages from mice and performed Western blot experiments. Initially, it was observed that SPP1 levels were notably increased in the Piezo1 knockdown group (Fig. 3E). Within the PI3K/AKT pathway, despite AKT levels being roughly constant, phosphorylated AKT (P-AKT) and downstream signaling molecule p-S6 were significantly elevated (Fig. 3E). This implies that in mice with Piezo1 knockdown, the PI3K/AKT pathway was significantly upregulated following LPS treatment. Our research has indicated that both the upregulation of SPP1 and the PI3K/AKT pathway can promote macrophage polarization towards the M2 phenotype, playing an anti-inflammatory role. We also verified changes in cardiac macrophage-derived inflammatory cytokines; in the hearts of Piezo1 knockdown mice, pro-inflammatory cytokines IL-1β and IL-6, primarily derived from M1 macrophages, were markedly decreased, whereas the anti-inflammatory cytokines IL-10, predominantly from M2 macrophages, were increased (Fig. 3F).

These changes reflect that the knockdown of Piezo1 activates the PI3K/AKT pathway, promotes the expression of SPP1, and causes macrophage polarization towards the M2 phenotype. Consequently, the anti-inflammatory protective capacity of macrophages is enhanced, inflammation levels are reduced, and cardiac function is protected (Fig. 3G).

Discussion

To examine the effects of myeloid cell-specific knockdown of Piezo1 on sepsis-induced cardiac dysfunction following LPS infection, our study employed a classical sepsis model induced by LPS, which ensured a mortality rate of 50–70% in mice. We successfully generated myeloid cell-specific Piezo1 knockdown mice to utilize within this framework. In these genetically modified mice, loss of Piezo1 conferred a markedly improved physiological state characterized by lower mortality rates, reduced weight loss, less cardiac edema, better cardiac function, and enhanced myocardial contractility after LPS infection. Histopathological findings further suggested that the diminishment of macrophage infiltration following Piezo1 deletion is likely attributable to Piezo1's regulatory role in macrophage proliferation and infiltration[21,22]. Additionally, upregulation of Piezo1 may lead to increased ROS production and cellular apoptosis[23]. Consequently, it can be inferred that the functional alterations in macrophages due to Piezo1 knockdown exerted a protective effect in mice. The postulate has been substantiated by HE staining and electron microscopy, which confirmed an improved condition of the myocardium after Piezo1 deletion. In this study, we do not have the Cre Recombinase-positive mice as a control group to determine the Cre-mediated toxicity phenotypes, has limitations. Previous studies[24] have shown that Cre-recombinase expression under the Lyz2 reporter influenced cell metabolics, independently of loxP site directed DNA recombination. And the Piezo1 deletion leading to decreased inflammatory response as a protective factor for sepsis, rather than causing disease, further in vitro studies are necessary to investigate Cre-mediated toxicity phenotypes.

Previous research has categorized macrophages into two subsets, M1 and M2[5], with M2 being associated with more pronounced anti-inflammatory effects[25,26]. We proceeded to assess macrophage polarization within our study. Initially, we conducted conventional morphological observations and flow cytometric analyses of bone

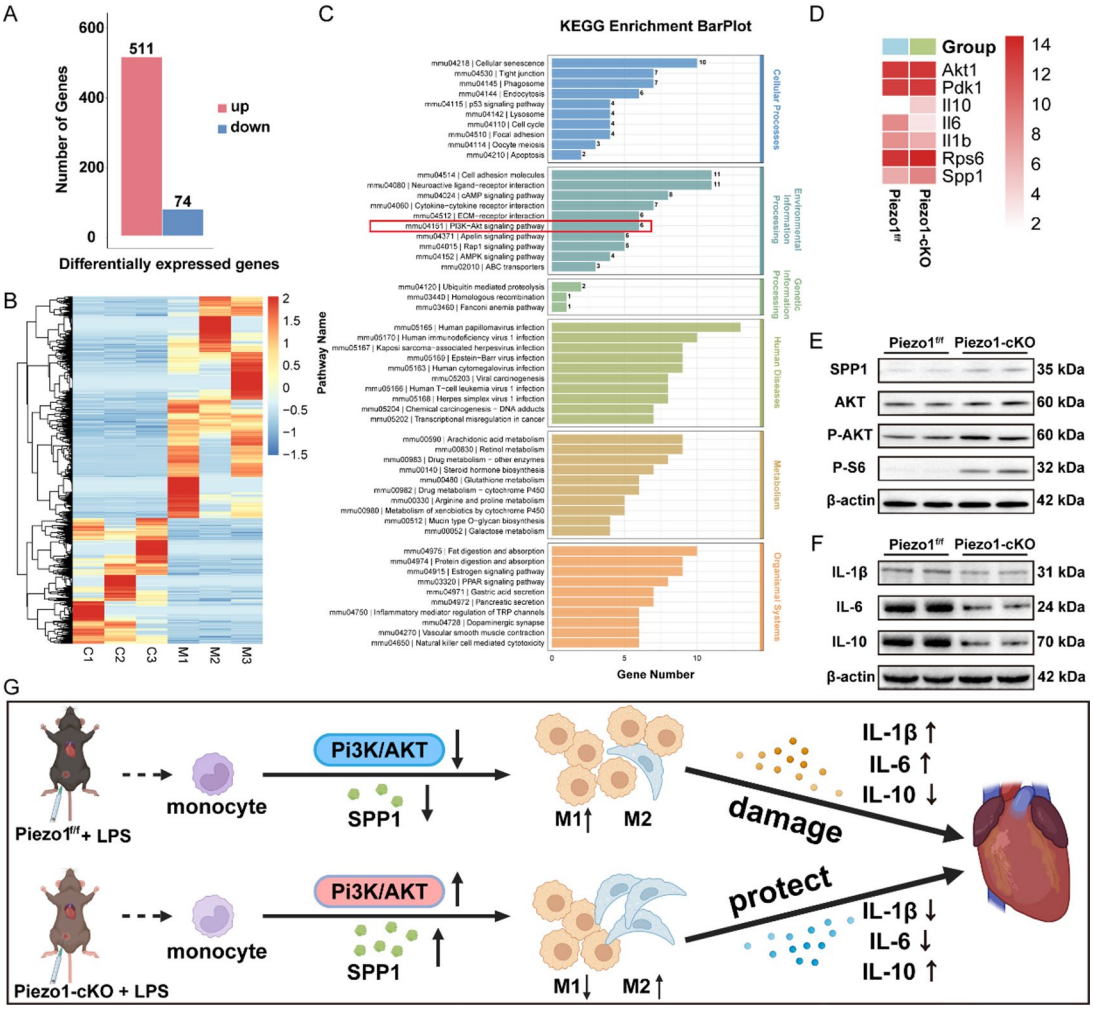

Fig. 3. Mechanism of Piezo1 knockdown macrophages in alleviating Sepsis-induced cardiomyopathy. (**A**) Differentially expressed genes in BMDMs from LPS-treated Piezo1-cKO and LPS-treated Piezo1$^{f/f}$ mice (n = 3). (**B**) Heatmap illustrating clustering of differential gene expression. (**C**) KEGG pathway enrichment analysis (Created with KEGG Database). (**D**) Heatmap visualizing differential gene expression. (**E**) Western blot results for bone marrow-derived macrophages from LPS-treated Piezo1-cKO and LPS-treated Piezo1$^{f/f}$ mice (n = 6). (**F**) Western blot results for cardiac tissue (LPS-treated Piezo1$^{f/f}$ and LPS-treated Piezo1-cKO mice, n = 6). (**G**) Conceptual diagram depicting cardioprotection mediated by Piezo1 knockdown-induced M2 macrophage polarization (Created in BioRender).

marrow-derived macrophages, which revealed an increase in the M2 macrophage population. Subsequently, immunofluorescence staining for macrophage subsets within the cardiac tissue demonstrated a significantly higher expression of CD206, an M2 marker. Based on these findings, we can tentatively conclude that Piezo1 may play a role in promoting the differentiation of macrophages towards the M2 phenotype.

To dissect the underlying mechanisms, we performed transcriptomic analysis on six mice and observed significant differences in gene expression following Piezo1 knockdown. SPP1, originally characterized as a pro-inflammatory cytokine secreted by T cells, is a multifunctional glycoprotein that is also expressed in an array of tissue-resident macrophages. This molecule plays a pivotal role in the phagocytic clearance of apoptotic cells, the chemotactic response, and the directed migration of macrophages[27]. A study highlights that SPP1 fosters M2 macrophage polarization through its interaction with αvβ3 integrin and CD44 receptors[17]. Notably, SPP1 and the PI3K/AKT pathway have been implicated in macrophage polarization in prior studies[28]. Some researchers have reported that a reduction in SPP1 correlates with a decrease in factors associated with M2 macrophage polarization, and others have considered SPP1 as a key target for macrophage phenotype identification and a prognostic factor for cancer outcomes[15,29]. Upon assessing protein expression changes, we discerned that Piezo1 knockdown resulted in upregulated expression of SPP1, accompanied by enhanced activation of the PI3K/AKT signaling pathway, both of which promote differentiation towards the M2 macrophage phenotype. The interplay between SPP1 and the PI3K/AKT pathway has been recognized in previous studies. One study in prostate cancer revealed that high SPP1 expression maintained PI3K/AKT pathway activation[30], while another study on bone fracture healing found that activation of the PI3K/AKT pathway stimulated M2 macrophage polarization[9].

Although we have verified that Piezo1 knockdown could cause the polarization of macrophages towards M2, this may also relate to the role of Piezo1 in stiffness sensing and subsequent regulation of macrophage polarization[31]. Moreover, Piezo1 knockdown appears to reduce the phagocytic activity of macrophages, which could be another consequence of the shift toward the M2 phenotype. We cannot exclude the possibility that this phagocytic reduction might inhibit polarization towards the M1 phenotype, contributing to an increased proportion of the M2 phenotype. To further elucidate the intricate mechanistic details, it may be necessary to conduct single-cell sequencing to analyze different cell types and to perform a more comprehensive dissection of the underlying processes.

Previous studies have authenticated the regulatory role of Piezo1 in modulating macrophage function and influencing the levels of inflammation[10,32,33]. Our study corroborated these findings by observing changes in myocardial inflammation, which align with the anti-inflammatory M2 macrophage phenotype. Specifically, the pro-inflammatory cytokines IL-1β and IL-6 were significantly diminished, whereas the anti-inflammatory cytokine IL-10 was elevated[13]. This pattern of cytokine expression indicates that myocardial cells were shielded from inflammatory damage, thereby exhibiting improved cardiac function. In our study, we chose to assess these cytokines in heart tissue instead of serum because a previous study[34] that evaluated both cardiac tissue and serum levels of IL-1β and IL-6 reported concordant expression patterns. Zhang et al.[35] demonstrated that LPS-induced septic mice exhibit simultaneous elevations of IL-6 and TNF-α in both serum and heart tissue, suggesting that serum measurements are suitable for systemic monitoring. However, tissue analysis provides a more direct assessment of local inflammatory intensity. In future work, we plan to include serum cytokine measurements to enhance the comprehensiveness of our study.

Our investigation indicates that Piezo1 knockdown in macrophages activates the PI3K/AKT pathway and drives the expression of SPP1, which in turn polarizes macrophages towards the M2 phenotype. Within myocardial tissues, these macrophage alterations not only lower inflammation levels but also boost their anti-inflammatory capacity, thereby conferring cardioprotection and preserving cardiac function in mice, suggesting Piezo1 might as a potential therapeutic target in clinical intervention.

Limitations and future perspectives

This study has several limitations that should be acknowledged. First, although macrophages were collected from Piezo1-cKO mice, it is important to note that the Lyz2 gene, utilized as the promoter for Cre-recombinase, is expressed not only in macrophages but also in other granulocyte populations. Therefore, it is essential to evaluate these additional granulocytes upon Piezo1 deletion to ensure the generalizability of the findings. Second, although echocardiographic assessments of LVEF and FS have been conducted in mice with heart rates maintained between 400 and 600 bpm, a more comprehensive approach to confirm cardiac dysfunction would involve measuring global longitudinal strain, and we will measure global longitudinal strain to confirm dysfunction in the future. Third, and perhaps most critically, this study did not analyze cardiac tissue resident macrophage cells; further in vitro and in vivo studies are necessary to investigate changes in infiltrating macrophage cells following LPS treatment, between the Piezo1-cKO and control mice.

Data availability

The data that support the findings of this study are available from the corresponding author upon reasonable request. The datasets generated and analysed during the current study are available in the GEO repository, under the accession number Nos. GSE311976, (www.ncbi.nlm.nih.gov/geo/).

Received: 24 May 2025; Accepted: 31 December 2025
Published online: 08 January 2026

References

1. Hollenberg, S. M. & Singer, M. Pathophysiology of sepsis-induced cardiomyopathy. *Nat. Rev. Cardiol.* **18**, 424–434. https://doi.org/10.1038/s41569-020-00492-2 (2021).
2. Atcha, H. et al. Mechanically activated ion channel Piezo1 modulates macrophage polarization and stiffness sensing. *Nat. Commun.* **12**, 3256. https://doi.org/10.1038/s41467-021-23482-5 (2021).
3. Liang, W. et al. Interleukin-5 deletion promotes sepsis-induced M1 macrophage differentiation, deteriorates cardiac dysfunction, and exacerbates cardiac injury via the NF-κB p65 pathway in mice. *BioFactors* **46**, 1006–1017. https://doi.org/10.1002/biof.1681 (2020).
4. Wang, Z. et al. Il12a deletion aggravates sepsis-induced cardiac dysfunction by regulating macrophage polarization. *Front. Pharmacol.* **12**, 632912. https://doi.org/10.3389/fphar.2021.632912 (2021).
5. McWhorter, F. Y., Wang, T., Nguyen, P., Chung, T. & Liu, W. F. Modulation of macrophage phenotype by cell shape. *Proc. Natl. Acad. Sci. U S A* **110**, 17253–17258. https://doi.org/10.1073/pnas.1308887110 (2013).
6. Li, D. et al. Maresin 1 alleviates the inflammatory response, reduces oxidative stress and protects against cardiac injury in LPS-induced mice. *Life Sci.* **277**, 119467. https://doi.org/10.1016/j.lfs.2021.119467 (2021).
7. Wu, A. H. & Feng, Y. J. Biochemical differences between cTnT and cTnI and their significance for diagnosis of acute coronary syndromes. *Eur. Heart J.* **19**(Suppl N), N25-29 (1998).
8. Geng, J. et al. TLR4 signalling via Piezo1 engages and enhances the macrophage mediated host response during bacterial infection. *Nat. Commun.* **12**, 3519. https://doi.org/10.1038/s41467-021-23683-y (2021).
9. Zhao, S. J. et al. Macrophage MSR1 promotes BMSC osteogenic differentiation and M2-like polarization by activating PI3K/AKT/GSK3β/β-catenin pathway. *Theranostics* **10**, 17–35. https://doi.org/10.7150/thno.36930 (2020).
10. Solis, A. G. et al. Mechanosensation of cyclical force by PIEZO1 is essential for innate immunity. *Nature* **573**, 69–74. https://doi.org/10.1038/s41586-019-1485-8 (2019).
11. Baratchi, S. et al. Transcatheter aortic valve implantation represents an anti-inflammatory therapy via reduction of shear stress-induced, piezo-1-mediated monocyte activation. *Circulation* **142**, 1092–1105. https://doi.org/10.1161/circulationaha.120.045536 (2020).

12. Aykut, B. et al. Targeting Piezo1 unleashes innate immunity against cancer and infectious disease. *Sci. Immunol.* **5**, eaab5168. https://doi.org/10.1126/sciimmunol.abb5168 (2020).
13. Shapouri-Moghaddam, A. et al. Macrophage plasticity, polarization, and function in health and disease. *J. Cell Physiol.* **233**, 6425–6440. https://doi.org/10.1002/jcp.26429 (2018).
14. Luo, S. et al. Piezo1 specific deletion in macrophage protects the progression of liver fibrosis in mice. *Theranostics* **13**, 5418–5434. https://doi.org/10.7150/thno.86103 (2023).
15. Zhang, Y., Du, W., Chen, Z. & Xiang, C. Upregulation of PD-L1 by SPP1 mediates macrophage polarization and facilitates immune escape in lung adenocarcinoma. *Exp. Cell Res.* **359**, 449–457. https://doi.org/10.1016/j.yexcr.2017.08.028 (2017).
16. Dong, B., Wu, C., Huang, L. & Qi, Y. Macrophage-related SPP1 as a potential biomarker for early lymph node metastasis in lung adenocarcinoma. *Front. Cell Dev. Biol.* **9**, 739358. https://doi.org/10.3389/fcell.2021.739358 (2021).
17. Yuan, Q. et al. MyD88 in myofibroblasts enhances colitis-associated tumorigenesis via promoting macrophage M2 polarization. *Cell Rep.* **34**, 108724. https://doi.org/10.1016/j.celrep.2021.108724 (2021).
18. Kanehisa, M., Furumichi, M., Sato, Y., Matsuura, Y. & Ishiguro-Watanabe, M. KEGG: Biological systems database as a model of the real world. *Nucleic Acids Res.* **53**, D672-d677. https://doi.org/10.1093/nar/gkae909 (2025).
19. Kanehisa, M., Sato, Y., Kawashima, M., Furumichi, M. & Tanabe, M. KEGG as a reference resource for gene and protein annotation. *Nucleic Acids Res.* **44**, D457-462. https://doi.org/10.1093/nar/gkv1070 (2016).
20. Kanehisa, M. & Goto, S. KEGG: Kyoto encyclopedia of genes and genomes. *Nucleic Acids Res.* **28**, 27–30. https://doi.org/10.1093/nar/28.1.27 (2000).
21. He, Y. et al. Myeloid Piezo1 deletion protects renal fibrosis by restraining macrophage infiltration and activation. *Hypertension* **79**, 918–931. https://doi.org/10.1161/hypertensionaha.121.18750 (2022).
22. Xu, H. et al. Mechanical force modulates macrophage proliferation via Piezo1-AKT-Cyclin D1 axis. *Faseb J.* **36**, e22423. https://doi.org/10.1096/fj.202200314R (2022).
23. Liu, H. et al. Dexamethasone upregulates macrophage PIEZO1 via SGK1, suppressing inflammation and increasing ROS and apoptosis. *Biochem. Pharmacol.* **222**, 116050. https://doi.org/10.1016/j.bcp.2024.116050 (2024).
24. Rahman, S. M. N., Yung, J. H. M., Volchuk, A., Goldenberg, N. M. & Giacca, A. Metabolic phenotypes in a Lyz2Cre recombinase mouse model. *Front. Immunol.* **16**, 1499858. https://doi.org/10.3389/fimmu.2025.1499858 (2025).
25. Wynn, T. A., Chawla, A. & Pollard, J. W. Macrophage biology in development, homeostasis and disease. *Nature* **496**, 445–455. https://doi.org/10.1038/nature12034 (2013).
26. Yao, Y., Xu, X. H. & Jin, L. Macrophage polarization in physiological and pathological pregnancy. *Front. Immunol.* **10**, 792. https://doi.org/10.3389/fimmu.2019.00792 (2019).
27. De Schepper, S. et al. Perivascular cells induce microglial phagocytic states and synaptic engulfment via SPP1 in mouse models of Alzheimer's disease. *Nat. Neurosci.* **26**, 406–415. https://doi.org/10.1038/s41593-023-01257-z (2023).
28. He, L. et al. Global characterization of macrophage polarization mechanisms and identification of M2-type polarization inhibitors. *Cell Rep.* **37**, 109955. https://doi.org/10.1016/j.celrep.2021.109955 (2021).
29. Bill, R. et al. CXCL9:SPP1 macrophage polarity identifies a network of cellular programs that control human cancers. *Science* **381**, 515–524. https://doi.org/10.1126/science.ade2292 (2023).
30. Pang, X. et al. SPP1 promotes enzalutamide resistance and epithelial-mesenchymal-transition activation in castration-resistant prostate cancer via PI3K/AKT and ERK1/2 pathways. *Oxid. Med. Cell. Longev.* **2021**, 5806602. https://doi.org/10.1155/2021/5806602 (2021).
31. Ma, S. et al. A role of PIEZO1 in iron metabolism in mice and humans. *Cell* **184**, 969-982.e913. https://doi.org/10.1016/j.cell.2021.01.024 (2021).
32. Lai, A. et al. Mechanosensing by Piezo1 and its implications for physiology and various pathologies. *Biol Rev Camb Philos Soc* **97**, 604–614. https://doi.org/10.1111/brv.12814 (2022).
33. Tang, Y. et al. Mechanosensitive Piezo1 protein as a novel regulator in macrophages and macrophage-mediated inflammatory diseases. *Front. Immunol.* **14**, 1149336. https://doi.org/10.3389/fimmu.2023.1149336 (2023).
34. Wu, L., Huang, J., Jia, X. & Mao, X. Role and mechanism of mitochondrial ribosomal proteins in septic myocardial injury. *J. Inflamm. Res.* **18**, 2677–2698. https://doi.org/10.2147/jir.S495987 (2025).
35. Svennerholm, K. et al. Escherichia coli outer membrane vesicles can contribute to sepsis induced cardiac dysfunction. *Sci. Rep.* **7**, 17434. https://doi.org/10.1038/s41598-017-16363-9 (2017).

Acknowledgements

The authors are thankful for the experimental platform provided by the State Key Laboratory of Cardiovascular Disease, China & Fuwai Hospital, Chinese Academy of Medical Sciences & Peking Union Medical College.

Author contributions

Y.H.Z., Y.Z., Y.J.T., and J.Y.S.: Writing—original draft, Visualization, Validation, Methodology, Investigation, Formal analysis, Conceptualization. Z.W.Z., W.H.J., and H.Z.: Investigation, Formal analysis. H.L.L., Y.B.M., and Z.W.N.: Writing—review & editing. Q.Z.G., S.L., J.Q.P., and T.Y.S.: Validation. Y.Z.W., B.H.P., M.H., C.Y.L., Z.L.L., and D.L.Z.: Writing—review & editing, Validation, Supervision, Resources, Project administration, Funding acquisition, Formal analysis, Conceptualization.

Funding

This research was supported by the National Natural Science Foundation of China (82300301), and Beijing Natural Science Foundation (7232077), and the Basic Research Project of Yunnan Provincial Science and Technology Department (202401AY070001-020), and the Basic Research Joint Special Program of the Yunnan Provincial Department of Science and Technology and Kunming Medical University (202401AY070001-019), and Noncommunicable Chronic Diseases-National Science and Technology Major Project (2024ZD0527500).

Declarations

Competing interests

The authors declare no competing interests.

Ethical approval and consent to participate

This study has been approved by the Institutional Committee on Animal Care of Capital Medical University

(Protocol number A5095F17-EA0D-4377-88F7-FED2CE3A2ED2).

Additional information

Supplementary Information The online version contains supplementary material available at https://doi.org/10.1038/s41598-025-34794-7.

Correspondence and requests for materials should be addressed to Z.L., Y.T., D.Z. or J.P.

Reprints and permissions information is available at www.nature.com/reprints.

Publisher's note Springer Nature remains neutral with regard to jurisdictional claims in published maps and institutional affiliations.